Prediction of Bond-Slip Behavior of Circular/Squared Concrete-Filled Steel Tubes

Rabab A. Allouzi [1,*] , **Hatem H. Almasaeid** [2] , **Donia G. Salman** [3] , **Raed M. Abendeh** [3] and **Hesham S. Rabayah** [3]

1   Department of Civil Engineering, The University of Jordan, Amman 11942, Jordan
2   Department of Civil Engineering, Al Albayt University, Al-Mafraq 25113, Jordan; almasaeid.h@aabu.edu.jo
3   Department of Civil and Infrastructure Engineering, Al-Zaytoonah University of Jordan, Amman 11733, Jordan;
     d.salman@zuj.edu.jo (D.G.S.); r.abendeh@zuj.edu.jo (R.M.A.); h.rabayah@zuj.edu.jo (H.S.R.)
*   Correspondence: r.louzi@ju.edu.jo; Tel.: +962-79-5288527

Abstract: Numerous existing formulas predicted the ultimate interfacial bond strength in concrete-filled steel tubes (CFST) between steel tubes and concrete core without investigating the whole response under push-out load. In this research, four models are proposed to predict the interfacial behavior in CFST including the post-peak branch under the push-out loading test based on 157 circular specimens and 105 squared specimens from the literature. Two models (one for circular and one for squared CFST) are developed and calibrated using artificial neural network (ANN) and two models (one for circular and one for squared CFST) are developed based on multivariable regression analysis, analysis of variance (ANOVA). The shape of the specimen (circular or squared), diameter of the tube, thickness of the tube, concrete compressive strength, age at the time of testing, and length of the specimen are the main factors considered. These models are then compared to other existing formulas to verify their capability to better predict the ultimate interfacial bond strength. It is found that the ANN model gives better results for most of the considered data. It is also found that ANN models can predict the overall bond-slip response for the considered dataset. In order to simulate the response of any CFST column using finite element (FE) method, it is vital to have sufficient input data on the overall bond-slip behavior between the interior face of the steel tube and the exterior surface of the concrete core including the post-peak branch. Accordingly, the suggested ANN model is used to generate the required input data related to the cohesive behavior and damage along the interface in ABAQUS model to simulate the response of two circular and two squared CFST columns under concentric compressive load. The results are in good agreement with experimental outcomes. The cohesive criterion and damage interface that are used based on ANN models in FE are found to be sufficient and can be adopted to model CFST columns.

Keywords: concrete-filled steel tubes; artificial neural networks; analysis of variance; bond-slip behavior; finite element method

1. Introduction

Concrete-filled steel tube (CFST) columns are widely used in high-rise buildings, underground infrastructures, and bridges due to their ductility and lower weight compared to reinforced concrete. Their implementation in engineering structures dates back to the 1950s [1]. The use of this composite action of steel and concrete in CFSTs has several advantages over using pure steel or reinforced concrete members. The steel tube acts as formwork for the concrete and provides confinement to the core concrete which enhances the strength and ductility of concrete. On the other hand, the concrete core provides stiffness and compressive strength to the steel tube which reduces the chances of local buckling taking place in steel tubes.

The behavior of the concrete-steel bond in CFSTs has been extensively investigated and tested by many researchers. It has been found that the bond strength is affected by the

cross-section geometry, shrinkage, age of concrete, interface roughness, compaction, and the use of lubrication [2–13].

The interfacial bond strength in CFSTs is obtained by using two methods: the push-off test and the push-out test. The loading is applied to the entire section in the push-off test, and this method can only test the ultimate bond strength [14]. On the other hand, many researchers used the push-out test because it assesses the bond strength between steel and concrete throughout the whole loading process [15,16]. The interfacial ultimate bond strength value is the main focus of these test methods.

Different equations have been proposed by researchers to predict this ultimate bond strength of CFSTs under push-out tests. Roeder et al. [7] conducted an experimental investigation on twenty circular CFSTs. The experimental program studied the bond behavior of CFST with a large diameter to thickness ratio (D/t) compared to other previous studies [4,5,17]. Parsely et al. [18] also proposed an equation to obtain the bond strength of square CFST based on eight squared specimens under push-out tests. The effects of the replacement level of recycled aggregate (δ), concrete compressive strength (f_{cu}), and length/diameter ratio (L_e/d) on the bond strength of circular recycled aggregate CFST were considered by Chen et al. [19].

Xue and Cai [20] investigated the bond strength based on thirty-two CFST specimens. It was concluded that interfacial bond strength is mainly attributed to the concrete strength, applied interfacial treatment, and the curing conditions of concrete. However, the interfacial length was found to be irrelevant to the bond strength.

Lyu and Han [21] proposed two empirical formulas to predict the ultimate bond strength for circular and square CFSTs. The proposed equations were based on a series of push-out tests on fifty-six CFST specimens with different cross-sectional types (circular and squared) and dimensions, interfacial treatment processes, and different replacement ratios of recycled coarse aggregate. It was recommended that to obtain the best predictions, the compressive strength value of concrete (f'_c) should be within 20–60 MPa. Additionally, the diameter or width be within 120–600 mm with the (D/t) ratio not to be more than 60.

The effect of shrinkage and creep that can develop in composite structures was studied by Martinelli [22]. The finite element solution was employed along the interfacial surface within a time integration procedure in order to account for the accumulation of strains due to these long-term effects. The models were validated based on experimental data.

It can be noticed through the literature, that there are many existing formulas to predict the ultimate bond strength. However, there is no available equation that can predict the post-peak behavior which is significant to investigate CFST columns under different loadings and can be used to provide input data for the concrete-steel interface in the finite element (FE) models.

In this study, interfacial bond-slip models are proposed for CFSTs including the initial branch till ultimate bond strength and the corresponding ultimate slip, in addition to the post-peak branch. The ultimate bond strength, its corresponding slip value, and the parameters required to define the post-peak exponent function are predicted using artificial neural network (ANN) and multivariable regression, the analysis of variance (ANOVA). The predictions are based on specimens previously tested under different parameters, such as concrete properties and CFST dimensions.

Calibrated finite element models of structural members can be used to estimate the behavior of these members under various conditions that they are not tested for. CFST is a structural member that needs to be calibrated so it can be further used to investigate its response under various conditions. In this paper, ABAQUS [23] is used to model previously tested CFST columns under axial loads. In order to simulate the performance of such columns, input data of the overall bond-slip behavior between the interior face of the steel tube and the exterior surface of the concrete core including the post-peak branch is essential. Accordingly, the bond-slip behavior based on the proposed ANN models are further used herein to generate the required input data related to the cohesive behavior and damage along the interface in ABAQUS models.

The behavior of CFSTs under push-out loading is mainly characterized by two stages; ascending branch and post-peak branch as shown in Figure 1a. The ascending branch is considered linear up to the average or ultimate bond strength (τ_u) and its corresponding slip value (S_u).
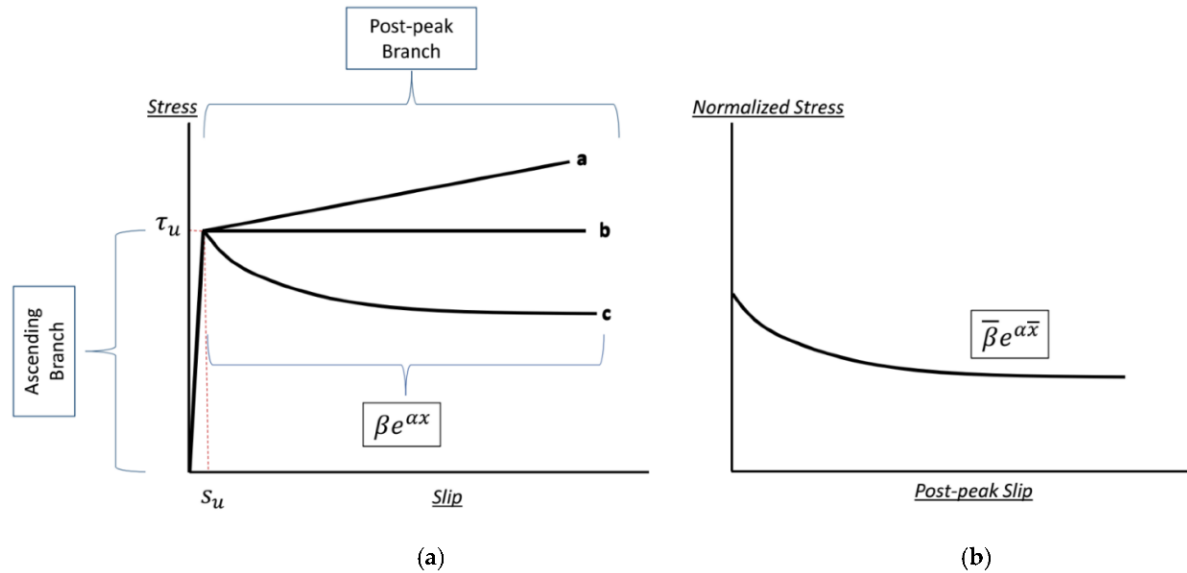
Figure 1. Idealized response curves of concrete-filled steel tubes (CFSTs) under push-out loading test to represent; (**a**) the overall behavior and (**b**) the normalized post-peak behaviour.

The average bond stress was commonly used by most of the researchers to indicate the bond strength in the push-out test regardless of the non-uniform interfacial bond stress distribution [4] and was defined as

$$\tau_u = \frac{p_f}{A_i} \tag{1}$$

where p_f is the maximum load which results in breaking the bond, and A_i is the interfacial area between the internal inner surface of the steel tube and the outer surface of the concrete core.

However, different definitions of bond strength were used in the literature, such as the peak bond stress or the post-peak residual bond stress. While the slip value (S_u) which corresponds to the ultimate bond strength represents the relative slip between the concrete core and the steel tube. Nevertheless, the slip results include both the relative slip between the infill concrete and the steel tube as well as the compressive deformations of the concrete and steel tube. However, because these compressive deformations have a small effect on the bond mechanism and strength, and because it is difficult to distinguish them from interfacial slip results due to the experimental conditions, only relative slip between infill concrete and steel tube was considered.

After reaching the peak bond strength (τ_u), the push-out curves through the literature were noticed to have three different trends for the post-peak behavior depending on the macro-dimensional deviations [24]. This trend can represent hardening, softening, or constant plasticity as indicated in Figure 1a by trends a, c, and b, respectively. No predictions were found in the literature to capture both the ascending and post-peak branches which form the whole behavior of the push-out test.

In this research, the softening trend is adopted to represent the post-peak behavior of CFSTs, and, as a result, only specimens that followed this trend are chosen for analysis. This post-peak branch is expressed as an exponential function using β and α parameters as presented by Equation (2).

$$y = \beta e^{\alpha x} \tag{2}$$

This branch is normalized against the ultimate bond strength and shifted to the origin point as shown in Figure 1b, so the equation becomes

$$\bar{y} = \bar{\beta} e^{\alpha \bar{x}} \tag{3}$$

2. Experimental Database

The circular and squared specimens considered in this study were chosen from twelve previous studies [5,6,11,18,21,24–31]. No treatment along the interfacial length between the concrete core and steel tube was provided such that the interaction between the two surfaces relied on the natural bond. Additionally, no shear connectors or studs were used in the considered specimens. Besides, the additives that replaced aggregates in the concrete mixture for some specimens were considered through the cubic compressive strength parameter, f_{cu}.

The considered variables of specimens were; diameter (D) or width (B) of the circular or squared specimen, respectively, the thickness of the steel tube (t), the interfacial length between the concrete and steel tube (L_i), the cubic strength of the concrete mixture (f_{cu}), and finally the age of the concrete mixture.

Tables S1 and S2 are included as supplementary documents that summarize the details of circular and squared specimens from literature and used in this study.

3. Analysis of Variance (ANOVA)

A multivariate linear analysis of variance (ANOVA) was carried out to calculate the parameters that represent the interfacial behavior, namely; τ_u, s_u, $\bar{\beta}$ and α for both circular and square CFSTs based on the aforementioned test results. To achieve the best predictions by applying these equations, it is recommended to use specimens with (L_i) less than 1200 mm and the concrete age (T) of not more than one year. The equations proposed for circular specimens are

$$\tau_u = 1.53623 + 0.00047D + 0.10393t - 0.00071L_i - 0.00585f_{cu} - 0.00173T \tag{4}$$

$$S_u = 1.00209 - 0.01305D + 0.26067t + 0.00033L_i + 0.01941f_{cu} + 0.00070T \tag{5}$$

$$\beta = 0.79605 + 0.00028D - 0.00223t + 0.00008L_i + 0.00153f_{cu} + 0.00026T \tag{6}$$

$$\alpha = -0.04938 + 0.00017D + 0.00006t + 0.00002L_i + 0.00009f_{cu} - 0.00018T \tag{7}$$

and for squared specimens are

$$\tau_u = 1.66240 - 0.00556B + 0.05539t - 0.00014L_i - 0.00792f_{cu} - 0.00123T \tag{8}$$

$$S_u = -1.95025 - 0.00033B + 0.30021t - 0.00327L_i + 0.11636f_{cu} - 0.00045T \tag{9}$$

$$\beta = 0.79707 + 0.00100B - 0.01877t - 0.00014L_i + 0.00248f_{cu} + 0.00028T \tag{10}$$

$$\alpha = -0.26698 - 0.00108B + 0.01067t + 0.00012L_i + 0.00568f_{cu} + 0.00028T \tag{11}$$

The τ_u, S_u, $\bar{\beta}$ and α results of ANOVA equations of circular and square CFSTs are listed in Tables S1 and S2 respectively. These results are also presented in Figure 2 for circular specimens and Figure 3 for squared specimens. By applying ANOVA analysis, the mean value (μ), standard deviation (σ), and R^2 of ($\tau_{u\ Exp.}/\tau_{u\ Pred.}$) are presented in Table 1. It is found that the ANOVA results compare well with the experimental results and the mechanical-based discussion is presented in Section 4. ANOVA is an efficient parametric method for analyzing experiment data since it is practical and adaptable [32]. However, it is a considerably complex and subtle method to use as there are numerous ANOVA variations, each of which corresponds to a specific experimental situation. As such, it is possible to use the wrong type of ANOVA for a given experimental situation and draw incorrect conclusions from the data [33].
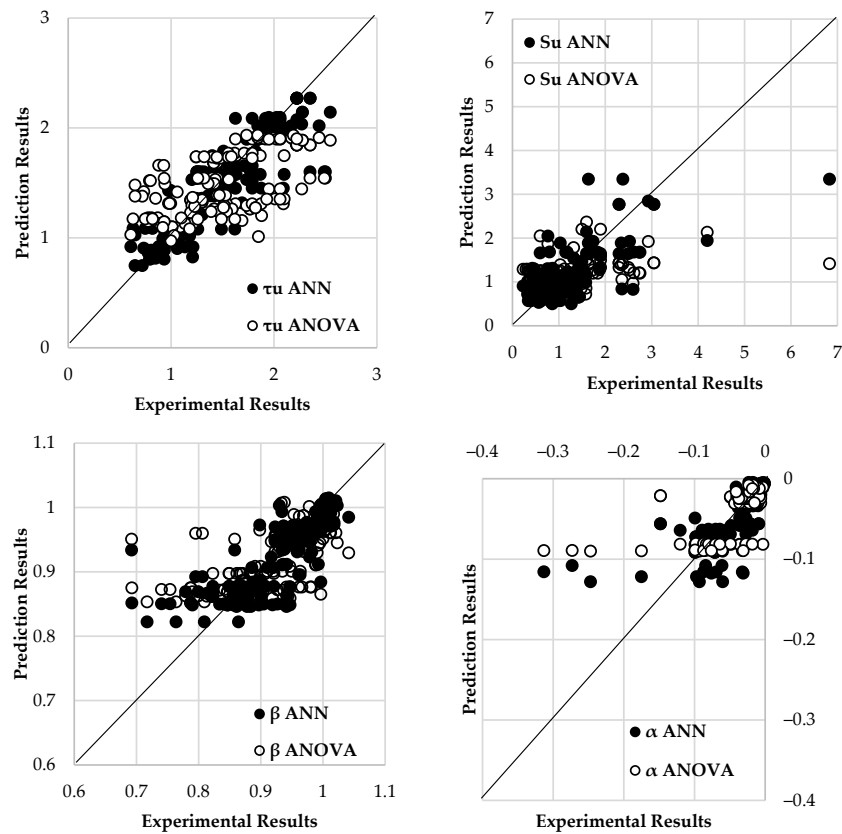
Figure 2. Predicted parameters using ANN and ANOVA vs. experimental results for circular specimens.
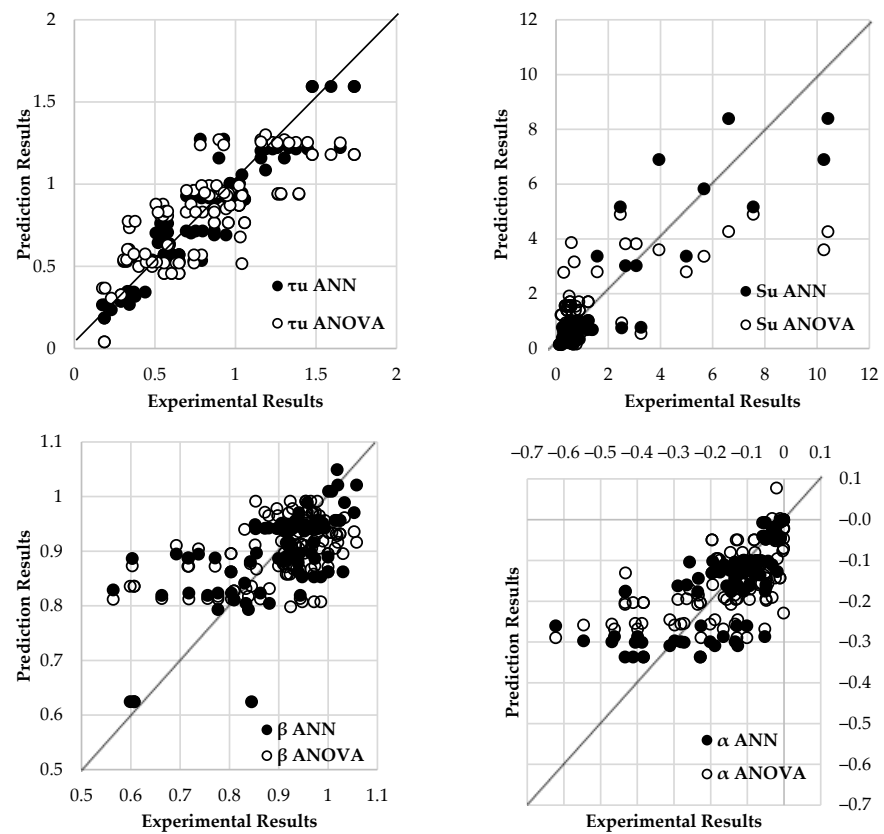

Figure 3. Predicted parameters using ANN and ANOVA vs. experimental results for squared specimens.

Table 1. Comparison between mean value, standard deviation, and R^2 of the ratio of experimental values to estimated values using the proposed ANOVA and ANN.

Shape	Output	ANN Results			ANOVA Results		
		Mean Value, μ	Standard Deviation, σ	R^2	Mean Value, μ	Standard Deviation, σ	R^2
Circular	τ_u (MPa)	0.999	0.166	0.876	1.001	0.277	0.328
	S_u (mm)	1.023	0.462	0.674	1.006	0.611	0.140
	β	1.000	0.052	0.742	1.000	0.062	0.394
	α	1.090	0.713	0.695	0.935	0.945	0.409
Square	τ_u (MPa)	1.004	0.188	0.837	1.067	0.596	0.623
	S_u (mm)	1.160	0.658	0.809	0.338	2.932	0.442
	β	1.000	0.096	0.570	1.000	0.117	0.231
	α	1.175	0.985	0.548	0.907	1.922	0.358

The predictions of this current study were based on specimens of various parameters that had been collected from various literature works then modeled using multivariate regression methods. Therefore, using ANOVA in this present study can be complicated because these parameters are correlated and affected by various factors. Accordingly, it is suggested to present another method of analysis for comparison. Machine Learning (ML) methods study links between inputs and outputs using statistical methods that enable computer systems to learn from a dataset without being explicitly programmed, which can be a good solution to this problem [34]. Several unique ML prediction methods have been used in recent decades. Artificial neural networks (ANNs) are one of them and are discussed further in the next section.

4. Artificial Neural Network (ANN)

It is vital to mention that several novel machine learning (ML) methods, i.e., artificial neural network (ANN), multi expression programming (MEP), and gene expression programming (GEP), have become very important forecasting and optimizing tools in many civil engineering fields. ML methods were introduced and utilized in predicting and modeling the non-linear behavior of different types of geoengineering materials like soil, concrete, asphalt, and clay which opened the door for revolutionary applications in the field of material science and optimization [35,36]. Additionally, ML methods can describe and recognize unnoticeable non-linear patterns among a high number of variables in extremely complex datasets due to the use of a non-linear activation function [37]. Moreover, ML has the advantage over regression in that the form of the model need not be pre-determined. ML was extensively utilized for predicting the mechanical behavior of concrete and concrete structural elements [38]. ML methods such as GEP were used to predict the ultimate load capacity of CFSTs [39]. On the other hand, ANN proved its ability to predict the mechanical properties of CFSTs such as the ultimate pure bending, the axial compression capacity, and fire performance [40–42].

In this study, the Feed-forward error Back-propagation (FB) method is utilized for calibrating the ANN models in this study. To model the behavior of CFST columns, two models are developed: ANN1 and ANN2 for circular and square columns, respectively. To develop the ANN models, 262 testing results datasets are utilized from the literature. These models are trained by utilizing the TRSEQ1 program, which was built on the FB algorithm [43]. The models are structured to have one hidden layer with a sigmoidal activation function.

ANN training can reflect efficient results if both inputs and outputs are normalized and scaled so the whole data vary from 0.1 to 0.9 before modeling. Once ANN models' inputs are scaled, the outputs are also be scaled, so the outputs are denormalized to give the results. Table 2 lists the parameters, maximum and minimum parameters values, and the ANN chosen maximum and minimum values for each parameter.

Table 2. Utilized datasets' maximum, minimum, ANN_{max}, and ANN_{min} values.

	Limit	f_{cu} (MPa)	Age (days)	L_i (mm)	T (mm)	B (mm)	D (mm)	τ_u (MPa)	S_u (mm)	$\bar{\beta}$	α
ANN1	Max	96.43	365	1095	6	-	219	2.55	6.83	1.04	-1×10^{-3}
	Min	9.11	28	190	2.5	-	107.7	0.61	0.23	0.69	-0.31
	ANN_{max}	120	450	1300	7	-	250	3	8	1.1	0
	ANN_{min}	0	0	0	1.5	-	75	0	0	0.6	-0.35
ANN2	Max	58.31	365	1498.6	6.6	254	-	1.74	10.42	1.06	-4×10^{-4}
	Min	9.11	28	190	3	90.85	-	0.17	0.13	0.5	-0.62
	ANN_{max}	70	450	1750	7.5	310	-	2	12.5	1.25	0
	ANN_{min}	0	0	0	1.75	30	-	0	0	0.3	-0.75

ANN_{max} and ANN_{min} values are chosen to be used in scaling the inputs and outputs so the scaled values are between 0.1 and 0.9 as shown in Equations (12) and (13). However, ANN models' prediction is restricted to be within the actual maximum and minimum values. Equations (12) and (13) are utilized in normalizing and denormalizing the data respectively.

$$\text{Normalized Parameter}_n = \frac{\text{Parameter}_n - ANN_{n_{min}}}{ANN_{n_{max}} - ANN_{n_{min}}} \tag{12}$$

$$\text{Parameter}_n = (\text{Normalized Value} \times (ANN_{n_{max}} - ANN_{n_{min}})) + ANN_{n_{min}} \tag{13}$$

The datasets utilized in ANN modeling are divided into three groups: training datasets, testing datasets, and validation datasets. Training datasets is utilized to optimize the network's connection links weights for different networks with a varying number of hidden nodes from 1 to 10. For each trained network, the statistical accuracy measurements; Average Squared Errors (ASE), Mean Absolute Relative Error (MARE), and coefficient of determination (R^2) are calculated and listed. The testing datasets are used to test the accuracy of the trained networks. The trained network with the lowest ASE value of the testing datasets is defined as the network with the optimum number of hidden nodes. After the optimization, both training and testing datasets are combined into one train-all datasets group and utilizedtoretrain the optimum network to get the connection links weights of the train-all model. Combining these two dataset groups allows the network to use more datasets in model training and capturing the relations between inputs and outputs which helps in increasing the model accuracy and reducing the error. The validation datasets (which were not used in training or testing the model) are utilized to check and validate the model by comparing them with the model's outputs.

Figure 4 illustrates a 5-n-4 (5 inputs, n hidden nodes, and 4 outputs) ANN model schematic. However, 5-n-4 ANN model mathematical equations can be written as in Equations (14) and (15).
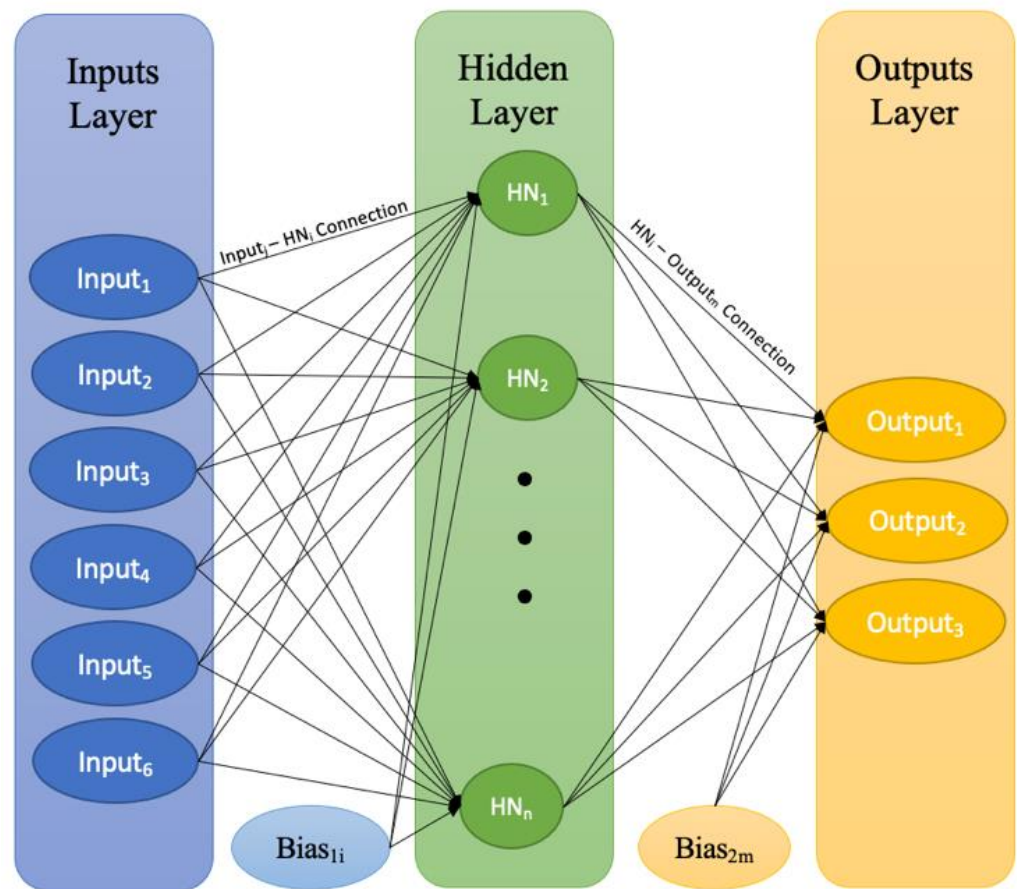
Figure 4. Schematic of 4 inputs, n hidden nodes, and 4 outputs ANN model.

$$Output_m = \frac{1}{1 + e^{-\sum_{i=1}^{n} HN_i \times (HN_i - Output_m Connection) + Bias_{2m}}} \tag{14}$$

$$HN_i = \frac{1}{1 + e^{-\sum_{j=1}^{5} Input_j \times (Input_j - HN_i Connection) + Bias_{1i}}} \tag{15}$$

The developed ANN models are:

1. ANN1 (for circular column): 157 datasets of circular columns are utilized. The datasets are divided into 117 training datasets, 30 testing datasets, and 10 validation datasets. ANN models' $ASE_{training}$, $ASE_{testing}$, $ASE_{train-all}$, and $ASE_{validation}$ values are listed in Figure 5a. Based on the values shown in Figure 5a, the optimum number of hidden nodes for ANN1 is found to be 9; because it has the lowest $ASE_{testing}$ value. Hence, ANN1 is denoted by its architecture as 5-9-4.

2. ANN2 (for square column): 105 datasets of circular columns are utilized. The datasets are divided into 75 training datasets, 20 testing datasets, and 10 validation datasets. As shown in Figure 5b, the optimum number of hidden nodes for ANN2 is found to be 7. So, ANN2 is denoted by its architecture as 5-7-4.

Figure 5 illustrates how combining testing and training datasets together and including them in the models training helps in reducing the ASE values and increasing the models' accuracy.

The connection links weights for ANN1 and ANN2 to be used in Equations (12) and (13) are shown in Tables 3 and 4, respectively. However, ANN modeling results are listed in Tables S1 and S2.
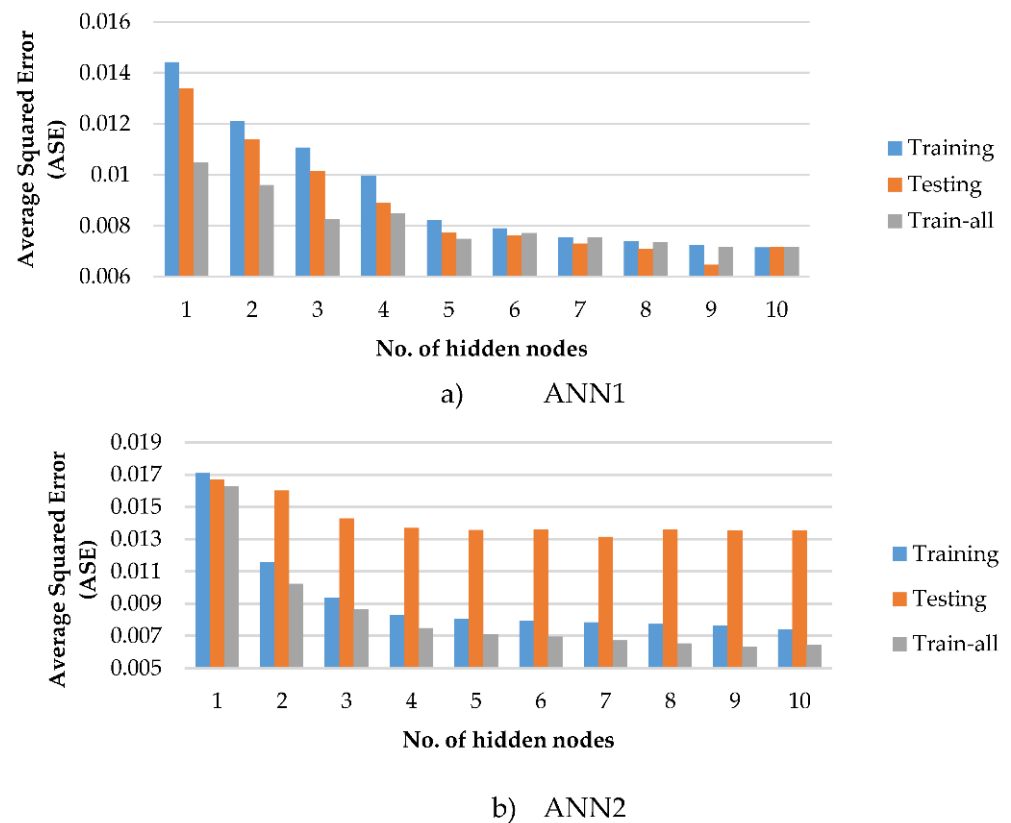
a)　　　ANN1

b)　ANN2

Figure 5. Average squared errors (ASE) values for networks with a different number of hidden nodes.

Table 3. Connection links weight used in 5-9-4 ANN1.

$Input_j$	Connection Links Weights between Inputs and Hidden Nodes ($Input_j$–HN_i Connection)								
	HN_1	HN_2	HN_3	HN_4	HN_5	HN_6	HN_7	HN_8	HN_9
$Input_1$ D (mm)	−11.17	−18.56	−20.95	−11.36	−8.69	−11.29	−2.26	−3.64	−2.72
$Input_2$ T (mm)	11.47	0.96	30.81	−8.25	−18.52	−7.72	−4.56	5.32	1.46
$Input_3$ L_i (mm)	−6.08	−15.98	0.44	−5.25	−4.93	−12.12	−4.70	−2.71	0.74
$Input_4$ f_{cu} (MPa)	−15.35	−15.39	1.55	−3.66	20.37	1.73	1.55	−5.55	0.90
$Input_5$ A (days)	−16.51	−0.93	−6.22	9.25	−0.62	−6.42	−2.36	−3.37	−3.67
$Bias_1$	5.26	11.98	−8.71	4.71	7.26	6.24	2.34	−0.84	−0.69

$Output_m$	Connection Links Weights between Hidden Nodes and Outputs (HN_i–$Output_m$ Connection)									
	HN_1	HN_2	HN_3	HN_4	HN_5	HN_6	HN_7	HN_8	HN_9	$Bias_2$
$Output_1$ τ_u (MPa)	4.28	−2.75	−3.64	1.46	0.65	6.97	−6.84	2.22	0.36	0.72
$Output_2$ S_u (mm)	−5.90	−0.84	7.19	3.65	3.37	2.21	−0.46	5.25	1.49	−5.70
$Output_3$ $\bar{\beta}$	−3.21	0.31	4.45	−0.11	1.36	2.51	0.19	−1.23	−3.11	0.20
$Output_4$ α	−5.13	3.49	3.70	−5.49	1.50	0.01	−1.90	−0.06	−0.06	2.44

Table 4. Connection links weight used in 5-7-4 ANN2.

Input$_j$	Connection Links Weights between Inputs and Hidden Nodes (Input$_j$–HN$_i$ Connection)							
	HN$_1$	HN$_2$	HN$_3$	HN$_4$	HN$_5$	HN$_6$	HN$_7$	
Input$_1$ B (mm)	3.49	−24.58	5.49	−7.53	−2.29	−1.42	−0.37	
Input$_2$ T (mm)	−11.94	10.40	−7.95	0.68	1.88	−2.02	−2.41	
Input$_3$ L_i (mm)	10.68	2.55	14.40	−0.92	−1.03	−1.43	−1.16	
Input$_4$ f_{cu} (MPa)	19.57	9.37	−0.57	8.37	−2.67	−6.08	0.00	
Input$_5$ A (days)	20.11	−6.96	14.91	0.27	5.37	−4.21	−0.42	
Bias$_1$	−11.30	−5.28	−4.33	−2.57	−1.66	1.15	−0.39	
Output$_m$	Connection Links Weights between Hidden Nodes and Outputs (HN$_i$–Output$_m$ Connection)							
	H1	H2	H3	H4	H5	H6	H7	Bias$_2$
Output$_1$ τ_u (N/mm^2)	−4.20	4.89	1.95	2.85	1.65	−0.75	−1.34	−0.19
Output$_2$ S_u (mm)	5.75	8.42	−6.37	−0.78	1.96	0.86	−0.81	−3.70
Output$_3$ $\bar{\beta}$	1.39	−7.36	−1.31	0.30	0.50	1.96	1.40	0.05
Output$_4$ α	12.72	16.91	−9.67	−1.06	−1.81	4.44	0.07	0.41

For both models, Table 5 lists the training, testing, train-all, and validation statistical accuracy measurements. However, Figure 4; Figure 5 show the experimental datasets versus the ANN prediction results of the validation results for ANN1 and ANN2 models respectively. Both validation statistical accuracy measurements (listed in Table 5) and the validation predicted versus experimental data results (shown in Figures 6 and 7) illustrate that ANN1 and ANN2 predictions are significantly reasonable and acceptable. Excel sheets of the ANN models are provided as supplementary documents.

Table 5. Statistical accuracy measurements of the developed ANN models.

| Model	5-9-4 ANN1 (Circular Column Model)	5-7-4 ANN2 (Square Column Model)
ASE$_{training}$	0.00724	0.007836
ASE$_{testing}$	0.006465	0.01313
ASE$_{train-all}$	0.007167	0.006721
ASE$_{validation}$	0.007048	0.007940
MARE$_{training}$	33. 648	41.586
MARE$_{testing}$	33.177	44.317
MARE$_{train-all}$	33. 229	39.400
MARE$_{validation}$	33.064	42.304
R$^2_{training}$	0.67767	0.59295
R$^2_{testing}$	0.54837	0.44174
R$^2_{train-all}$	0.74671	0.691078
R$^2_{validation}$	0.75730	0.631577
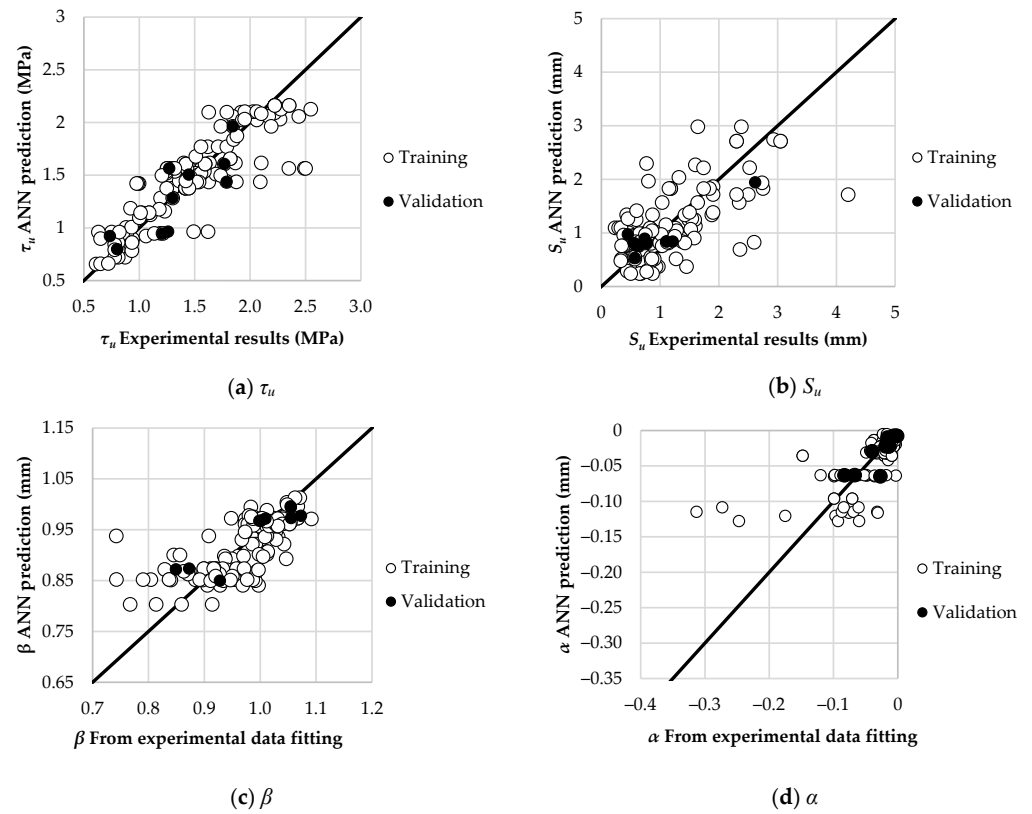
Figure 6. Training and validation results of the 5-9-4 ANN1 model versus experimental data.
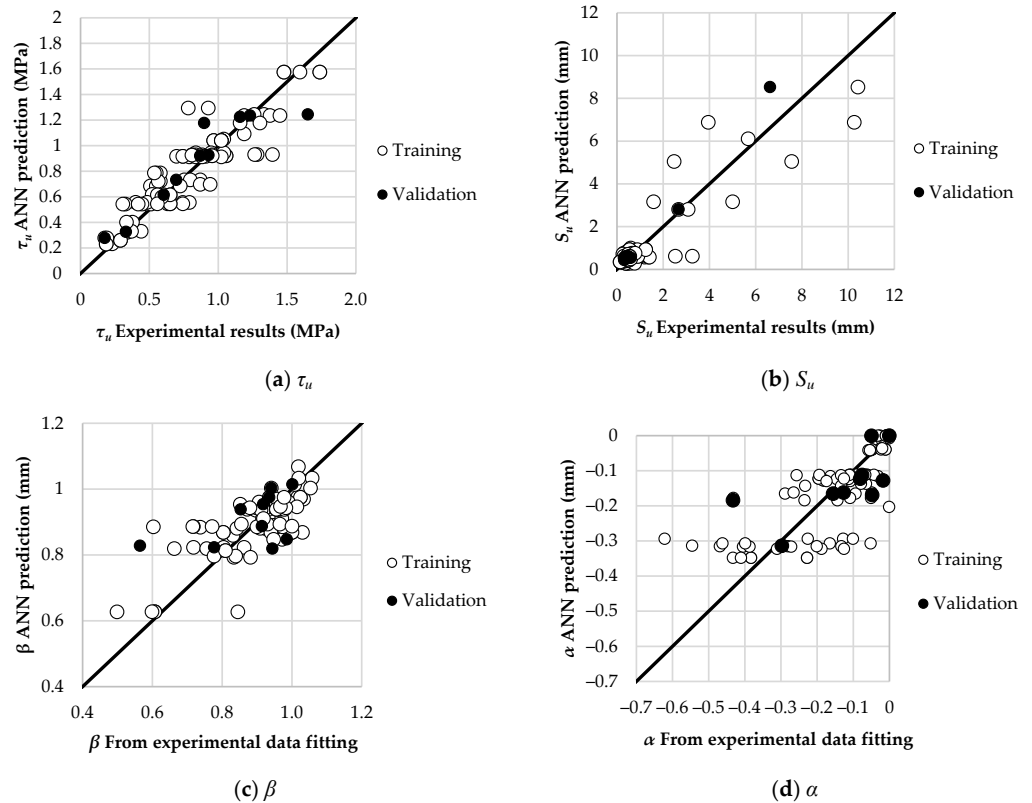

Figure 7. Comparison and discussion of results.

5. Comparison and Discussion of Results

5.1. Comparison of Bond Strength (τ_u) Predicted by ANOVA and ANN with Existing Models

Results of τ_u based on proposed equations in this paper and equations from literature for circular CFSTs of Roeder et al. [7], Xue and Cai [20], Lyu and Han [21], and Chen et al. [19] and equations for squared CFSTs of Parsley et al. [18], Lyu and Han [21], and Xue and Cai [20] are compared. It can be concluded that results by ANOVA and ANN proposed models can better represent most of the specimens compared to available equations. Mean values (μ) and standard deviation (σ) results estimated by ANOVA and ANN formulas and by the existing models are presented in Table 6.

Table 6. Comparison among mean value, standard deviation, and R^2 regarding the ultimate bond strength.

References	Prediction Model	Mean Value, μ	Standard Deviation, σ
Circular CFST			
Roeder et al. [7]	$\tau_u = 2.109 - 0.026(D/t)$	1.197	0.524
Xue and Cai [20]	$\tau_u = 0.1(f_{cu})^{0.4}$	4.316	1.809
Lyu and Han [21]	$\tau_u = 0.071 + 4900(t/D^2)$	1.212	0.549
Chen et al. [19]	$\tau_u = [0.0336 + 0.0141\delta - 0.0028(L_e/d)]f_{cu}$	2.487	1.414
Proposed ANOVA		1.001	0.277
Proposed ANN		0.999	0.1660
Squared CFST			
Parsley et al. [18]	$\tau_u = 0.013 + 1751(t/b^2)$	1.417	0.679
Lyu and Han [21]	$\tau_u = 0.043 + 1100(t/B^2)$	2.019	0.937
Xue and Cai [20]	$\tau_u = 0.1(f_{cu})^{0.4}$	2.544	1.255
Proposed ANOVA		1.067	0.596
Proposed ANN		1.004	0.188

5.2. Comparisons of τ_u, S_u, $\overline{\beta}$ and α Predicted by ANOVA and ANN for Both Circular and Squared CFSTs

It is found that most predicted values of τ_u, S_u, $\overline{\beta}$ and α by ANN models are closer to the experimental than ANOVA results (Table 1). ANN outperforms the ANOVA and provides more accurate prediction results due to the use of the sigmoidal activation function which allows the ANN to capture the non-linear mechanical behavior of concrete.

Figure 8 shows the total interfacial behavior obtained experimentally of one circular and one squared specimen versus the predicted behavior using ANN and ANOVA analysis. These two specimens were previously investigated by Abendeh et al. [26] The results also confirms that the ANN analysis can better represent the bond-slip behavior of CFSTs. Proposed excel sheets for predicting the entire bond-slip behavior of circular and squared CFSTs by using ANN are available as supplementary documents. Figures 9 and 10 present the whole experimental and predicted interfacial behavior (based on ANN models) of 6 circular specimens and 6 squared specimens, respectively. These specimens are selected from the different references adopted in this study to verify the capability of ANN models to represent the whole experimental bond-slip curves. For all predicted curves, the first point, after the ultimate bond strength is reached, on the post-peak curve is selected at S_u plus standard deviation.
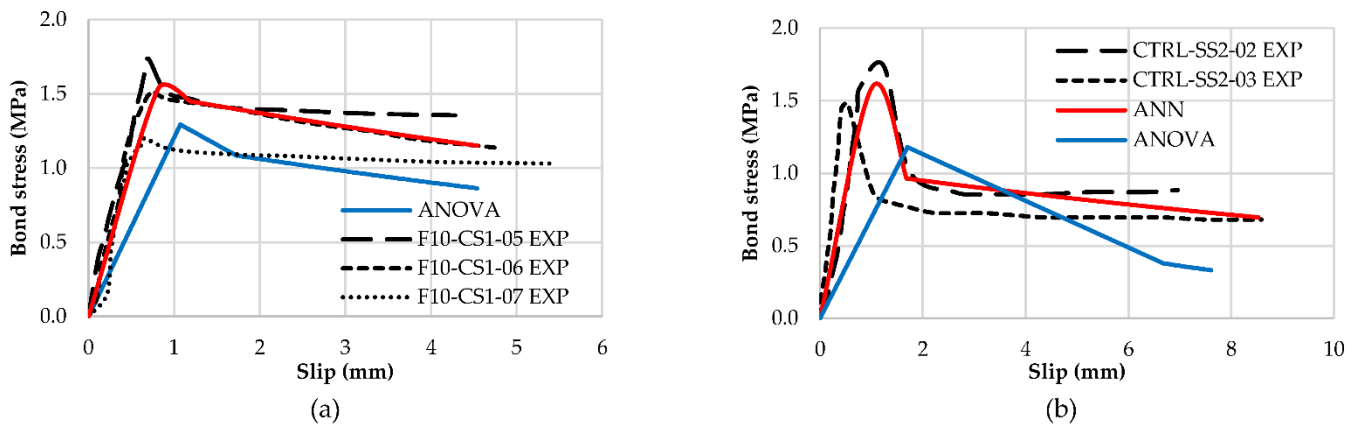
Figure 8. Experimental versus predicted interfacial behavior using ANN and ANOVA analysis of (**a**) circular and (**b**) squared specimens.
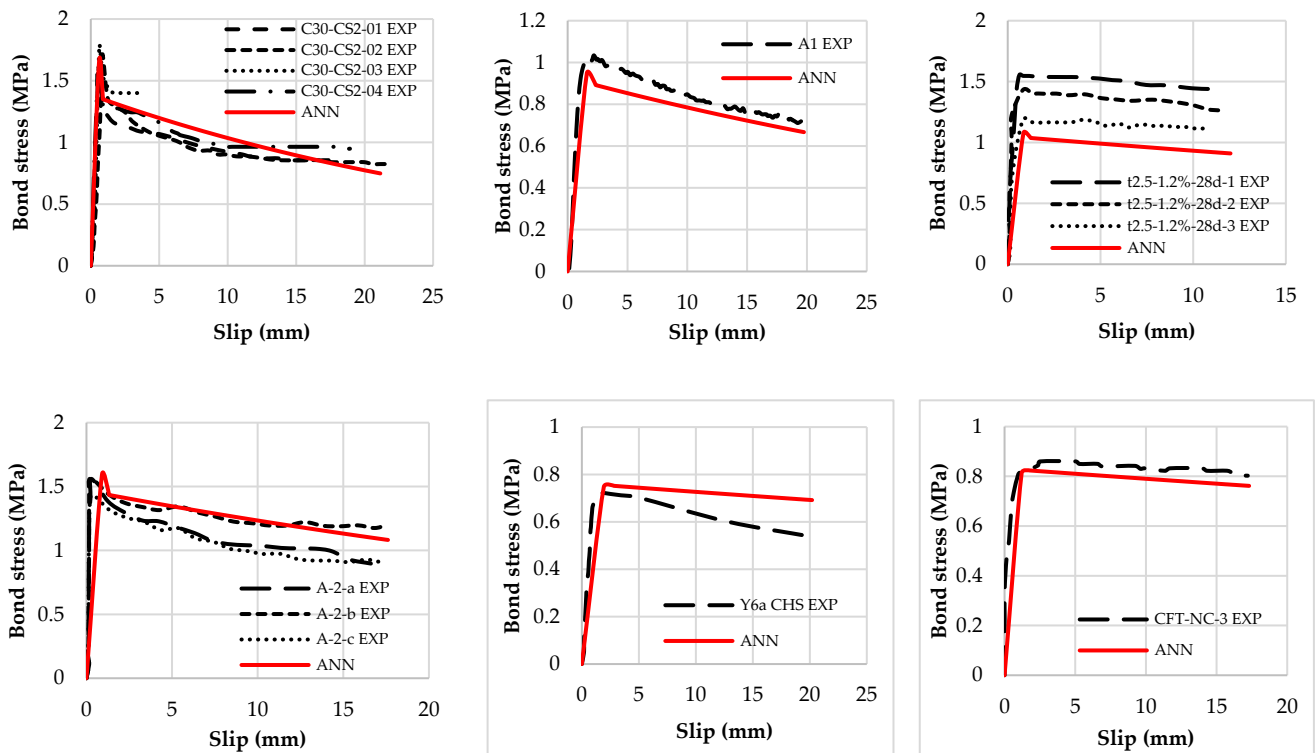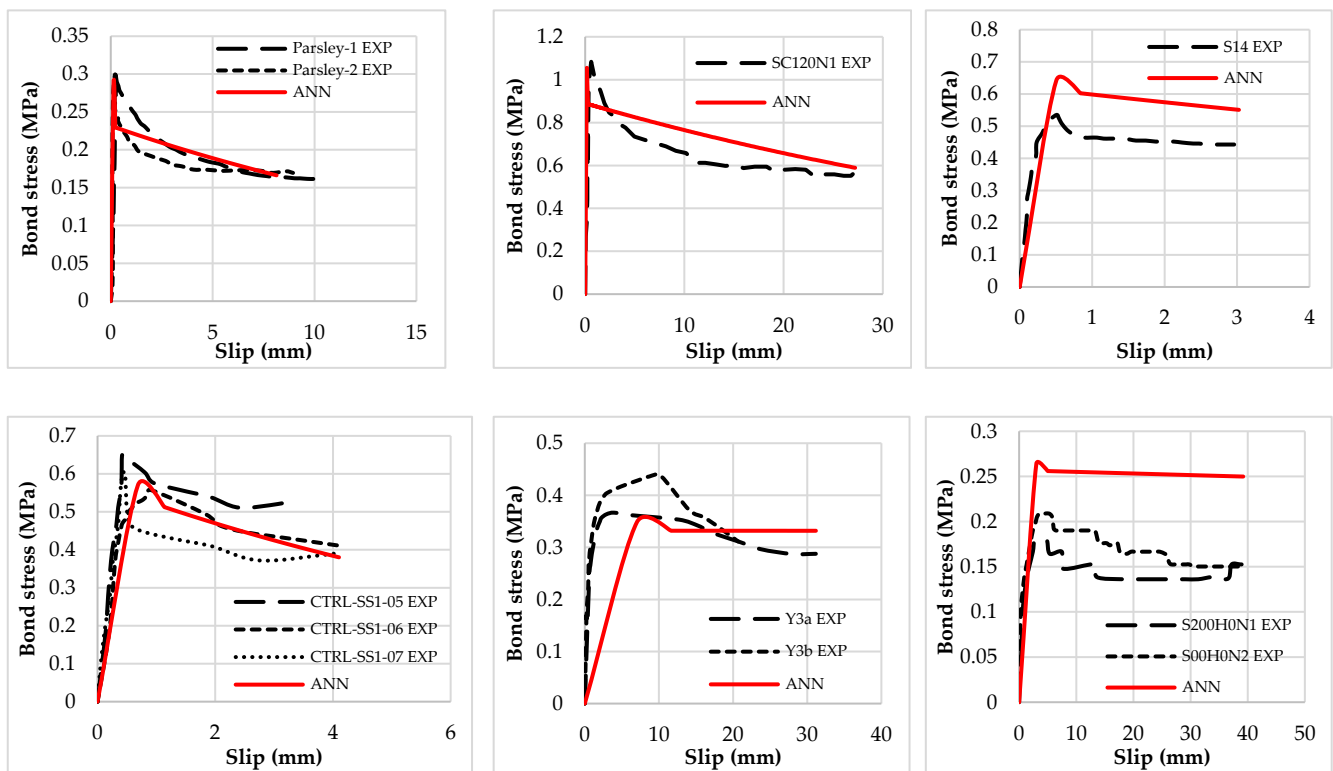

Figure 9. Experimental versus predicted interfacial behavior using ANN of circular specimens.

Figure 10. Experimental versus predicted interfacial behavior using ANN of squared specimens.

It should be stated that the proposed bond-slip behavior model (Figure 1) follows what was observed in the literature; the bond stress increase linearly, till the maximum bond stress value is reached. At this stage, no separation is seen in the interface between the concrete core and steel tubes. Hence, as both materials still work together, chemical adhesion dominates the bond resistance. Furthermore, the micro-interlocking forces increase with an increase in the push-out load. However, the macro-interlocking force does not contribute since no slip occurred between the various materials.

After reaching the peak, three kinds of curves are noted based on the macro-dimensional deviation [21,24]. The macro-interlocking force is produced from the confinement of steel tubes that prevented lateral expansion. It is also directly correlated to the size effect, which is produced by lateral expansion in concrete or the presence of irregularities in the internal surfaces of the steel tubes. Additionally, this force increases with an increase in the separation and relative slip. When the macro-dimensional deviation is large, the increase in friction is higher compared to the reduction in the initial friction. This leads to a hardening trend. On the other hand, if this friction value is lower compared to the reduction, the curve shows a softening trend. In intermediary situations, the curve showed a constant plasticity trend.

The difference between predicted and experimental results is considered reasonable since the test results of identical specimens encountered such a difference due to variation of properties of concrete, manufacturing, and previously mentioned irregularities in internal forces. For example, Figures 9 and 10 present the difference in τ_u of the three identical t2.5-1.2%-28d specimens, in S_u of the three identical CTRL-SS1 specimens, in β and α of the two identical specimens of Parsley.

6. Finite Element Modeling of CFST's Columns

In this paper, ABAQUS is used to model previously tested CFST columns under axial loads. The development of such models involves the discretization of components, the selection of the materials' constitutive models, and the approach to defining the interaction along the interfaces.

To develop calibrated finite element models of CFST members, it is vital to quantify and qualify the interaction characteristics along the concrete-steel interface. Abu Shamah and Allouzi [44] defined a surface to surface contact between the core-concrete and the steel tube using a shear stress limit according to Han et al. [45]. After the shear stress limit is reached, the softening behavior is not considered. The importance to identify the concrete-steel interface model was emphasized by Effendi [46]. Interface element and contact analysis were used along the interface and it was found that this method is better than rigid bar elements since rigid bar elements artificially add stiffness to the system. Nguyena et al. [47] investigated the use of the tie and slip contact properties between concrete and steel tubes. It was found that the tie model represented the test outcomes better than the slip model. Neither the tie model nor the slip model represents the actual interaction along the concrete-steel interface. Alatshan and Mashiri [48] defined the friction coefficient along the interface between the concrete and steel tube. The magnitude of this coefficient was reviewed from the literature.

The ANN models developed in this paper are used to define the interaction along the steel-concrete interface of simulated CFST columns.

6.1. Experimental Data for Calibration

Four CFST columns are developed using ABAQUS to verify if the proposed ANN models of the concrete-steel interaction can be used to simulate the interface characteristics along the concrete-steel interface of these columns. The details of these columns are presented in Table 7.

Table 7. Details of the specimens used for calibration.

References	Shape	Specimen	*D* (mm)	*t* (mm)	*L* (mm)	f'_c (MPa)	f_y (MPa)
Huang et al. [1]	circular	SA	108	4	324	43.9	336
		MA	108	4	1296	43.9	336
Huang et al. [49]	square	SU-40	200	5	600	27.15	265.8
		SU-70	280	4	600	31.15	272.6

6.2. Finite Element Discretization

Concrete and steel are modeled as 8-noded 3D elements. The mesh size adopted to model specimens "SA" and "MA" is 8 mm. A larger mesh size of 25 mm is used to model specimens "SU-40" and "SU-70" due to the larger sections of these specimens. As supports are modeled as a rigid body, the mesh size has no effect; accordingly, a mesh size of 20 mm is used.

6.3. Constitutive Models of Materials

The Concrete Damaged Plasticity model available in ABAQUS [23] is used which is a continuum model to represent the behavior of brittle materials such as concrete. This model involves tension and compression plasticity.

The input data of plasticity of concrete under compression is defined based on Tsai's equation [50] as

$$y = \frac{nx}{1 + \left(n - \frac{r}{r-1}\right)x + \frac{x^r}{r-1}} \tag{16}$$

where $x = \frac{\varepsilon_c}{\varepsilon'_c}$, $y = \frac{f_c}{f'_c}$. The strain at the compressive strength f'_c (in MPa) is taken as $\varepsilon'_c = \frac{f'_c}{4690 + 260 f'_c}$ [51]. n and r are parameters to control the shape of the stress-strain curve and are taken as $\frac{E_c \varepsilon'_c}{f'_c}$ and $\frac{f'_c}{5.2} - 1.9$, respectively [52].

The plasticity of concrete under tension is modeled based on Tsai's equation as

$$y = \frac{nx}{1 + \left(n_t - \frac{r}{r-1}\right)x + \frac{x^r}{r-1}} \tag{17}$$

where $x = \frac{\varepsilon_t}{\varepsilon_{t0}}$, $y = \frac{f_t}{f_{t0}}$. n_t and r are parameters to control the shape of the curve. The strain at peak tensile strength (f_t) is ε_{t0}.

For the concrete plasticity definition, the dilation angle of 22° is adopted. The flow potential eccentricity is taken as 0.1 and the ratio of biaxial to uniaxial compressive strength is taken as 1.16. The invariant stress ratio is 0.667 and the viscosity is 0.001.

An elastic-plastic model is used to simulate the steel tube.

6.4. Tube-Core Interface

Cohesive behavior is implemented between steel tube and concrete core, and it is represented based on traction versus separation law. Damage is also enforced to simulate the post-peak behavior in cohesion over two steps; damage initiation and damage evolution.

Damage initiation is selected based on the quadratic criterion of contact stress ratios that is represented based on ABAQUS manual [23] as

$$\left(\frac{t_n}{t_n^o}\right)^2 + \left(\frac{t_s}{t_s^o}\right)^2 + \left(\frac{t_t}{t_t^o}\right)^2 = 1 \tag{18}$$

where t_n, t_s, t_t are the contact stresses and t_n^o, t_s^o, t_t^o are the peak values of the contact stresses.

When the damage initiation criterion is met, the damage evolution is defined based on tabulated values of damage ratios versus slip displacement after the peak bond strength. The proposed ANN models presented in this paper define the bond-slip behavior of concrete-filled steel tube after bond strength that can be used to define damage evolution. The damage, d, is calculated as

$$d = 1 - \frac{\tau}{\tau_u} \tag{19}$$

where τ is the bond stress at specific slip displacement after the peak bond strength.

6.5. Finite Element Results

The axial load versus axial displacement curves of the four axial specimens are estimated using ABAQUS [23]. The measured versus numerically calculated responses of these specimens are shown in Figure 11. As shown in this figure, the simulated models can represent the experimental results very well for columns "SA" and "MA". Note that the length of column "MA" exceeds the maximum length of the data of circular specimens used to develop the ANN models and this can be the reason for the difference between numerical and experimental results. For columns "SU-40" and "SU-70", the results can represent the measured experimental results well and it is expected to get even better results if the steel constitutive model is tri-linear but the details of steel material were not provided in the reference. This verifies that the used cohesive criterion and damage based on the ANN models are sufficient and can be adopted to model CFST's columns under axial load.
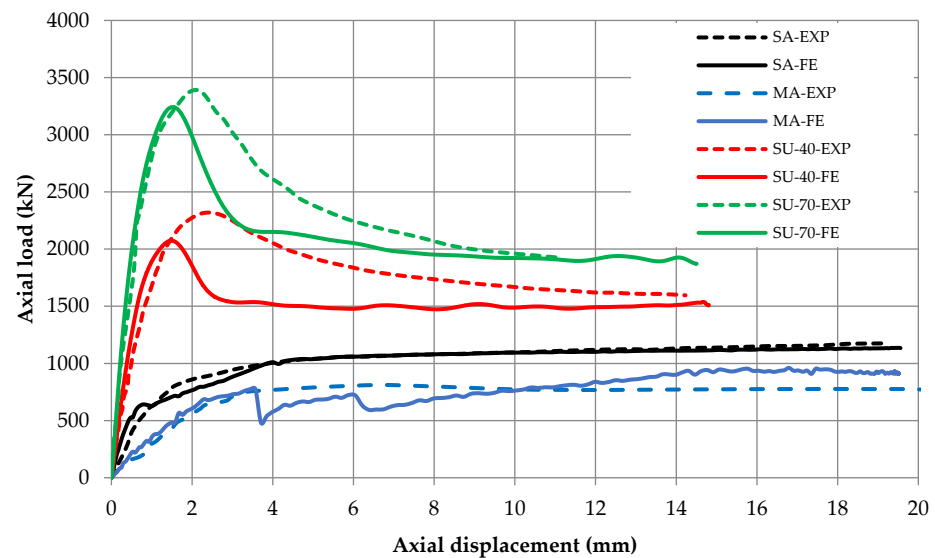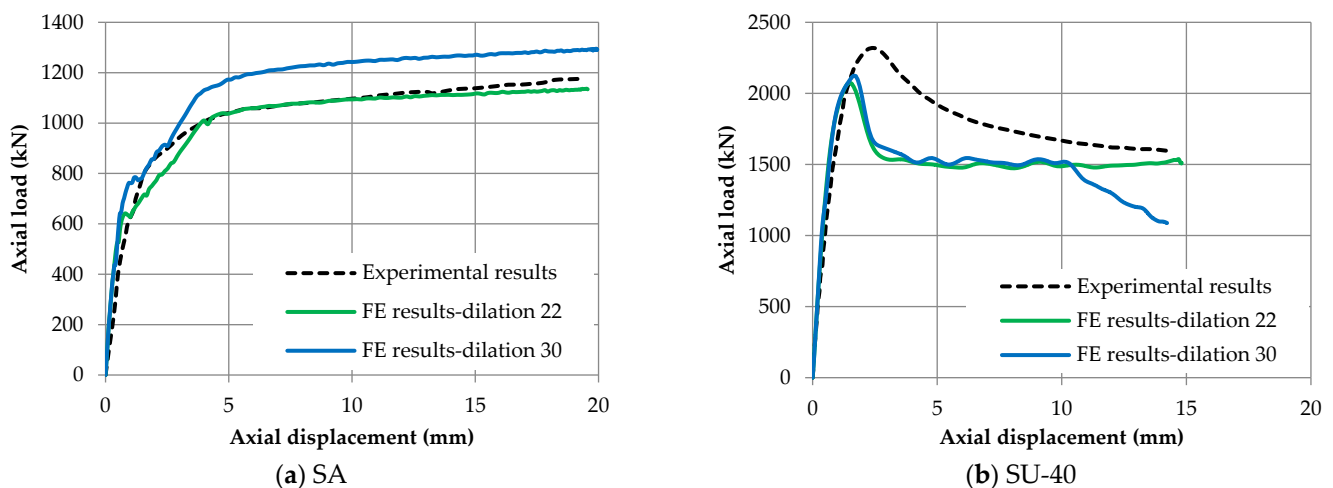
Figure 11. Load-deflection curves of the simulated models.

6.6. Sensitivity Analysis

The sensitivity of the results of finite element modeling to the input parameters is essential to study since it shows the effectiveness of the model and accordingly the outcomes. The main input parameters that are investigated for sensitivity are; the mesh size of steel tube and concrete and the dilation angle of concrete.

The dilation angle of concrete is the angle of internal friction and it controls the amount of plastic volumetric strain. For the definition of the concrete constitutive model, the dilation angle usually is selected based on the value that can represent the experimental response of one specimen and verify it for the other specimens [53]. The load-deflection results of specimens SA and SU-40 that are simulated with dilation angles of 22° and 30° are presented in Figure 12. It is found the circular column is more sensitive to the dilation angle value compared to the squared section.

(**a**) SA

(**b**) SU-40

Figure 12. Load-deflection curves of the simulated specimens using different dilation angles.

A mesh convergence study is performed where each column is simulated with different mesh sizes and the results are compared. Sufficiently small elements are used. Three mesh sizes are adopted to model specimens "SA" and "MA", namely; 8 mm, 15 mm, and 20 mm. Three mesh sizes are used to model specimens "SU-40" and "SU-70", namely; 15 mm, 20 mm, and 25 mm. The results of load-deflection of all considered columns at these

different mesh sizes are introduced in Figure 13. It is found that the peak load results are not affected by the different mesh sizes.
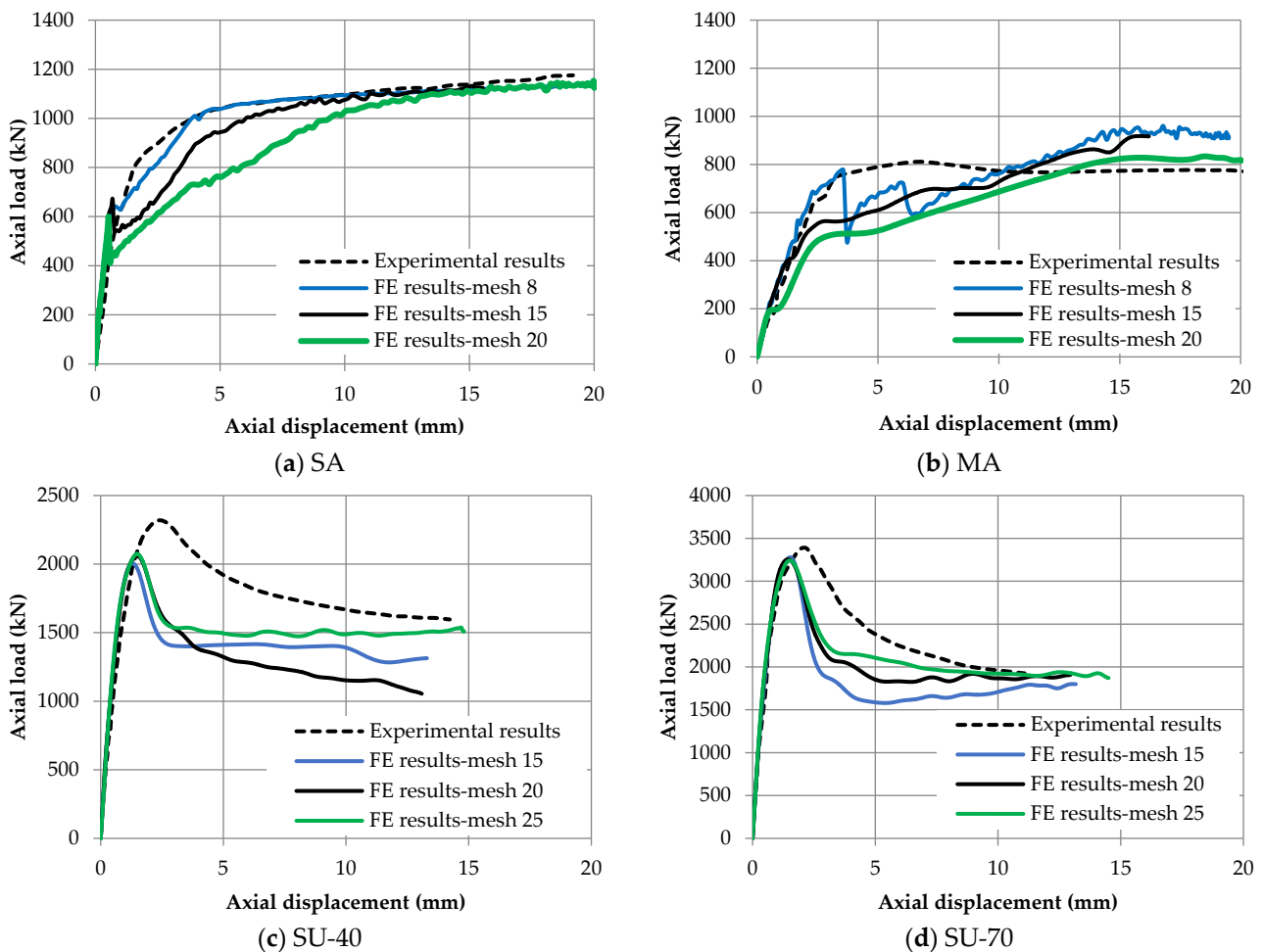
(a) SA

(b) MA

(c) SU-40

(d) SU-70

Figure 13. Load-deflection curves of the models simulated at different mesh sizes.

7. Conclusions

Concrete-Filled Steel Tube (CFST) columns are composite columns that are getting significant attention as a replacement for reinforced concrete due to their ductility and lower weight. CFST consists of an outer steel tube that is filled with concrete. Various models available in the literature are limited to predicting the ultimate bond strength along the steel-concrete interface of CFSTs under push-out loading. Nevertheless, there is no prediction of the post-peak behavior in the literature. Accordingly, the behavior along the steel-concrete interface in composite columns is investigated in this paper to propose prediction models of the overall behavior which can be used for engineering practice.

The dataset considered for this investigation includes 157 circular specimens and 105 squared specimens from several references. These specimens had the following key parameters; diameter or width that ranges from 90.85 mm to 254 mm, thickness that ranges from 2.5 mm to 6.6 mm, length that ranges from 190 mm to 1498.6 mm, core-concrete compressive strength that ranges from 9.11 MPa to 96.43 MPa, and age of concrete when the push-out test was performed that ranges from 28 days to 365 days.

ANN and ANOVA models are proposed in this study to obtain the overall stress-slip behavior of the CFSTs. The ANN analysis is shown to be the most appropriate models for anticipating overall interfacial behavior among the major existing equations and the suggested ANOVA formulas herein. The ratios of the experimental to the predicted ultimate bond strength based on ANOVA and ANN formulas have mean values of 1.001 and 0.999,

respectively for circular CFSTs, and 1.067 and 1.004, respectively for squared CFSTs. These mean values represent how ultimate bond strength is well predicted compared to the mean values of the results estimated by the other existing formulas. Moreover, the proposed ANOVA and ANN formulas have a standard deviation of 0.277 and 0.166, respectively, for circular specimens and 0.596 and 0.188, respectively, for squared specimens compared to the standard deviation values of the results estimated by the existing models. Hence, ANOVA and ANN are more appropriate models to predict the ultimate bond strength for circular and squared CFSTs.

The proposed ANN models provide better prediction results than ANOVA due to the use of the sigmoidal activation function which allows the ANN to capture the non-linear mechanical behavior of concrete. ANN models have a lesser standard deviation of the ratios of the experimental to the predicted ultimate bond strength, slip at ultimate bond strength, and the parameters controlling the post-peak curve. R^2 values are found ranging from 0.674 to 0.876 for circular CFSTs and from 0.548 to 0.837 for squared CFSTs, which are high compared to ANOVA results. Consequently, it can be concluded that ANN models are appropriate to anticipate the full behavior of circular and square CFSTs and are better than ANOVA.

The difference between ANN results and experimental outcomes is considered reasonable since the test results of identical specimens had similar differences in their slip-bond response curves. This can be attributed to the variation of properties of concrete, manufacturing, and previously mentioned irregularities in internal forces.

This paper also investigates the ability of proposed ANN models to be used in numerical non-linear finite element models to predict the performance of CFST's columns under axial load. It is concluded that calibrated finite element models can represent the experimental results which may make it beneficial to further study CFST's columns. The Concrete Damage Plasticity model and cohesive-damage interface based on ANN models are sufficient and can be adopted to simulate the behavior of CFST's columns under axial load.

Author Contributions: Conceptualization, R.A.A., H.H.A., D.G.S., R.M.A. and H.S.R.; methodology, R.A.A., H.H.A., D.G.S., R.M.A. and H.S.R.; software, R.A.A., H.H.A. and H.S.R.; validation, R.A.A., H.H.A. and H.S.R.; formal analysis, R.A.A., H.H.A., D.G.S., R.M.A. and H.S.R.; investigation, R.A.A., H.H.A., D.G.S., R.M.A. and H.S.R.; data curation, H.H.A., D.G.S. and R.M.A.; writing—original draft preparation, R.A.A., H.H.A., D.G.S. and R.M.A.; writing—review and editing, R.A.A., H.H.A., D.G.S. and R.M.A.; visualization, R.A.A., H.H.A. and D.G.S.; supervision, D.G.S. and R.M.A.; project administration, R.A.A. and R.M.A. All authors have read and agreed to the published version of the manuscript.

Institutional Review Board Statement: Not applicable.

Informed Consent Statement: Not applicable.

Data Availability Statement: Data is contained within the article or Supplementary Material.

References

1. Huang, F.; Yu, X.; Chen, B. The structural performance of axially loaded CFST columns under various loading conditions. *Steel Compos. Struct.* **2012**, *13*, 451–471. [CrossRef]
2. Virdi, K.S.; Dowling, P.J. *Bond Strength in Concrete Filled Circular Steel Tubes*; Composite columns. CESLIC Report. CC11; Engineering Structures Laboratories, Civil Engineering Department, Imperial College London: London, UK, 1975.
3. Morishita, Y. Experimental studies on bond strength in concrete filled square and octagonal steel tubular columns subjected to axial loads. *Trans. Jpn. Concr. Inst.* **1979**, *1*, 359–366.
4. Tomii, M.; Yoshimura, K.; Morishita, Y. A method of improving bond strength between steel tube and concrete core cast in circular steel tubular columns. *Trans. Jpn. Concr. Inst.* **1980**, *2*, 319–326.
5. Shakir-Khalil, H. Pushout strength of concrete-filled steel hollow sections. *Struct. Eng.* **1993**, *71*, 230–233.
6. Shakir-Khalil, H. Resistance of concrete-filled steel tubes to pushoutforces. *Struct. Eng.* **1993**, *71*, 234–243.
7. Roeder, C.W.; Cameron, B.; Brown, C.B. Composite Action in Concrete Filled Tubes. *J. Struct. Eng.* **1999**, *125*, 477–484. [CrossRef]
8. Kilpatrick, A.E.; Rangan, B.V. Influence of interfacial shear transfer on behavior of concrete-filled steel tubular columns. *Struct. J.* **1999**, *96*, 642–648.
9. Han, L.-H.; Yang, Y.-F. Influence of Concrete Compaction on the Behavior of Concrete Filled Steel Tubes with Rectangular Sections. *Adv. Struct. Eng.* **2001**, *4*, 93–100. [CrossRef]
10. Xu, C.; Chengkui, H.; Decheng, J.; Yuancheng, S. Push-out test of pre-stressing concrete filled circular steel tube columns by means of expansive cement. *Constr. Build. Mater.* **2007**, *23*, 491–497. [CrossRef]
11. Aly, T.; Elchalakani, M.; Thayalan, P.; Patnaikuni, I. Incremental collapse threshold for pushout resistance of circular concrete filled steel tubular columns. *J. Constr. Steel Res.* **2010**, *66*, 11–18. [CrossRef]
12. Tao, Z.; Han, L.-H.; Uy, B.; Chen, X. Post-fire bond between the steel tube and concrete in concrete-filled steel tubular columns. *J. Constr. Steel Res.* **2011**, *67*, 484–496. [CrossRef]
13. Qu, X.; Chen, Z.; Nethercot, D.A.; Gardner, L.; Theofanous, M. Load-reversed push-out tests on rectangular CFST columns. *J. Constr. Steel Res.* **2013**, *81*, 35–43. [CrossRef]
14. Tahir, M.M.; Shek, P.N.; Tan, C.S. Push-off tests on pin-connected shear studs with composite steel–concrete beams. *Constr. Build. Mater.* **2009**, *23*, 3024–3033. [CrossRef]
15. Chen, L.; Dai, J.; Jin, Q.; Chen, L.; Liu, X. Refining bond–slip constitutive relationship between checkered steel tube and concrete. *Constr. Build. Mater.* **2015**, *79*, 153–164. [CrossRef]
16. Yan, J.-B.; Liew, J.Y.R.; Sohel, K.M.A.; Zhang, M.H. Push-out tests on J-hook connectors in steel–concrete–steel sandwich structure. *Mater. Struct.* **2013**, *47*, 1693–1714. [CrossRef]
17. Virdi, K.S.; Dowling, P.J. Bond Strength in Concrete Filled Steel Tubes. *IABSE Proc.* **1980**, *4*, 125–139.
18. Parsley, M.A.; Yura, J.A. Push-out behavior of rectangular concrete-filled steel tubes. *Spec. Publ.* **2000**, *196*, 87–108.
19. Chen, Z.H.; Qu, X.S.; Wang, X.D.; Sun, R.R.; Li, L.M. Experimental Study on the Interface bearing capacity on concrete-filled square steel tube. *J. Harbin Inst. Technol.* **2009**, *41*, 27–32.
20. Xue, L.H.; Cai, S.H. Bond strength at the interface of concrete-filled steel tube columns. *Build. Sci.* **1996**, *12*, 22–28.
21. Lyu, W.-Q.; Han, L.-H. Investigation on bond strength between recycled aggregate concrete (RAC) and steel tube in RAC-filled steel tubes. *J. Constr. Steel Res.* **2019**, *155*, 438–459. [CrossRef]
22. Martinelli, E. A general numerical model for simulating the long-term response of two-layer composite systems in partial interaction. *Compos. Struct.* **2020**, *257*, 112929. [CrossRef]
23. Dassault Systèmes Simulia Corp. *ABAQUS Analysis User's Manual Online Documentation, Version (6.11)*; Dassault Systemes Simulia, Inc.: Providence, RI, USA, 2011; Available online: http://130.149.89.49:2080/v6.11/books/usb/default.htm (accessed on 30 March 2022).
24. Fu, Z.Q.; Ge, H.B.; Ji, B.H.; Chen, J.J. Interface bond behaviour between circular steel tube and lightweight aggregate concrete. *Adv. Steel Constr.* **2018**, *14*, 424–437. [CrossRef]
25. Ahmad, H.; Raed, S.; Abendeh, M.; Hunaiti, Y.M. Evaluation of concrete–steel interfaces in steel tubes filled with chipped rubber–concrete. *Proc. Inst. Civil Eng. Struct. Build.* **2020**, 1–23. [CrossRef]
26. Abendeh, R.; Ahmad, H.S.; Hunaiti, Y.M. Experimental studies on the behavior of concrete-filled steel tubes incorporating crumb rubber. *J. Constr. Steel Res.* **2016**, *122*, 251–260. [CrossRef]
27. Ke, X.; Sun, H.; Yang, Z. Calculation on bond strength of high-strength concrete filled steel tube. In *2015 4th International Conference on Sensors, Measurement and Intelligent Materials*; Atlantis Press: Shenzhen, China, 2016; pp. 995–999. [CrossRef]
28. Lu, Y.; Liu, Z.; Li, S.; Tang, W. Bond behavior of steel-fiber-reinforced self-stressing and self-compacting concrete-filled steel tube columns for a period of 2.5 years. *Constr. Build. Mater.* **2018**, *167*, 33–43. [CrossRef]
29. Lv, J.; Zhou, T.; Du, Q.; Li, K.; Jin, L. Research on the Bond Behavior of Preplaced Aggregate Concrete-Filled Steel Tube Columns. *Materials* **2020**, *13*, 300. [CrossRef]
30. Tao, Z.; Song, T.-Y.; Uy, B.; Han, L.-H. Bond behavior in concrete-filled steel tubes. *J. Constr. Steel Res.* **2016**, *120*, 81–93. [CrossRef]
31. Zou, W.; Liang, J.; Zhang, G.; Yang, H. Bond Properties of RAC-Filled Square Steel Tubes after High Temperature. *Adv. Mater. Sci. Eng.* **2019**, *2019*, 2413613. [CrossRef]
32. Armstrong, R.A.; Slade, S.V.; Eperjesi, F. An introduction to analysis of variance (ANOVA) with special reference to data from clinical experiments in optometry. *Ophthalmic Physiol. Opt.* **2000**, *20*, 235–241. [CrossRef]

33. Armstrong, R.A.; Eperjesi, F.; Gilmartin, B. The application of analysis of variance (ANOVA) to different experimental designs in optometry. *Ophthalmic Physiol. Opt.* **2002**, *22*, 248–256. [CrossRef]

34. Samuel, A.L. Some Studies in Machine Learning Using the Game of Checkers. *IBM J. Res. Dev.* **1959**, *3*, 210–229. [CrossRef]

35. El Tabach, E.; Lancelot, L.; Shahrour, I.; Najjar, Y. Use of artificial neural network simulation metamodelling to assess groundwater contamination in a road project. *Math. Comput. Model.* **2007**, *45*, 766–776. [CrossRef]

36. Javed, M.F.; Farooq, F.; Memon, S.A.; Akbar, A.; Khan, M.A.; Aslam, F.; Alyousef, R.; Alabduljabbar, H.; Rehman, S.K.U.; Rehman, S.K.U.; et al. New Prediction Model for the Ultimate Axial Capacity of Concrete-Filled Steel Tubes: An Evolutionary Approach. *Crystals* **2020**, *10*, 741. [CrossRef]

37. Manasrah, A.; Masoud, M.; Jaradat, Y.; Bevilacqua, P. Investigation of a Real-Time Dynamic Model for a PV Cooling System. *Energies* **2022**, *15*, 1836. [CrossRef]

38. Ilyas, I.; Zafar, A.; Javed, M.F.; Farooq, F.; Aslam, F.; Musarat, M.A.; Vatin, N.I. Forecasting Strength of CFRP Confined Concrete Using Multi Expression Programming. *Materials* **2021**, *14*, 7134. [CrossRef]

39. Farooq, F.; Ahmed, W.; Akbar, A.; Aslam, F.; Alyousef, R. Predictive modeling for sustainable high-performance concrete from industrial wastes: A comparison and optimization of models using ensemble learners. *J. Clean. Prod.* **2021**, *292*, 126032. [CrossRef]

40. Basarir, H.; Elchalakani, M.; Karrech, A. The prediction of ultimate pure bending moment of concrete-filled steel tubes by adaptive neuro-fuzzy inference system (ANFIS). *Neural Comput. Appl.* **2019**, *31*, 1239–1252. [CrossRef]

41. Tran, V.-L.; Thai, D.-K.; Nguyen, D.-D. Practical artificial neural network tool for predicting the axial compression capacity of circular concrete-filled steel tube columns with ultra-high-strength concrete. *Thin-Walled Struct.* **2020**, *151*, 106720. [CrossRef]

42. Moradi, M.; Daneshvar, K.; Ghazi-Nader, D.; Hajiloo, H. The prediction of fire performance of concrete-filled steel tubes (CFST) using artificial neural network. *Thin-Walled Struct.* **2021**, *161*, 107499. [CrossRef]

43. Najjar, Y.M. *Quick manual for TR-SEQ1*; Dept. of Civil Engineering, Kansas State University: Manhattan, KS, USA, 1999.

44. Abu-Shamah, A.; Allouzi, R. Numerical investigation on the response of circular double-skin concrete-filled steel tubular slender columns subjected to biaxial bending. *Steel Compos. Struct. Int. J.* **2020**, *37*, 533–549. [CrossRef]

45. Han, L.-H.; Yao, G.-H.; Tao, Z. Performance of concrete-filled thin-walled steel tubes under pure torsion. *Thin-Walled Struct.* **2007**, *45*, 24–36. [CrossRef]

46. Effendi, M.K. The Effect of Concrete-Steel Interface Model on Finite Element Analysis of Concrete Filled Square Steel Tube Beam. *Civ. Eng. J.* **2020**, *29*, 135–146. [CrossRef]

47. Nguyen, D.H.; Hong, W.-K.; Ko, H.-J.; Kim, S.-K. Finite element model for the interface between steel and concrete of CFST (concrete-filled steel tube). *Eng. Struct.* **2019**, *185*, 141–158. [CrossRef]

48. Alatshan, F.; Mashiri, F.R. Finite element modeling of concrete-filled steel tubes: Review and recent developments. In *Applied Mechanics and Materials*; Trans Tech Publications Ltd.: Baech, Switzerland, 2013; Volume 330, pp. 894–899. [CrossRef]

49. Huang, C.S.; Yeh, Y.-K.; Liu, G.-Y.; Hu, H.-T.; Tsai, K.C.; Weng, Y.T.; Wang, S.H.; Wu, M.-H. Axial Load Behavior of Stiffened Concrete-Filled Steel Columns. *J. Struct. Eng.* **2002**, *128*, 1222–1230. [CrossRef]

50. Tsai, W.T. Uniaxial Compressional Stress-Strain Relation of Concrete. *J. Struct. Eng.* **1988**, *114*, 2133–2136. [CrossRef]

51. Popovics, S. A review of stress-strain relationships for concrete. *J. Proc.* **1970**, *67*, 243–248.

52. Chang, G.A.; Mander, J.B. *Seismic Energy Based Fatigue Damage Analysis of Bridge Columns: Part 1–Evaluation of Seismic Capacity*; NCEER Technical Rep. No. NCEER-94-0006; University of Buffalo, The State University of New York: Buffalo, NY, USA, 1994.

53. Li, X.-X.; Wang, C.; Sato, J. Framework for dynamic analysis of radioactive material transport packages under accident drop conditions. *Nucl. Eng. Des.* **2019**, *360*, 110480. [CrossRef]